International Journal of Computer Information Systems and Industrial Management Applications
ISSN 2150-7988 Volume 17 (2025) pp. 546-564

Article

Construction of a Dynamic Monitoring and Early Warning System for Voltage Stability in Transparent Grids with High-Density Distributed Power Sources Based on Long Short-Term Memory Networks

Zhongqiang Zhou *, Tian Xia, Jianwei Ma, Ling Liang and Huijiang Wan

Power dispatching control center of Guizhou Power Grid Co., Ltd, Guiyang 550000, Guizhou, China;
dongfang10708@163.com

Abstract: With the large-scale integration of high-density distributed generation (DG) into distribution grids, the randomness and volatility of their output pose severe challenges to grid voltage stability. Traditional static analysis methods based on physical models struggle to meet the demands of real-time dynamic monitoring and early warning. Leveraging the real-time and efficient acquisition of power data through transparent grids, this paper proposes a voltage stability assessment method for high-density DG integration into transparent grids. This method employs a graph convolutional network (GCN), a bidirectional long short-term memory (BiLSTM) network, and an attention mechanism. Case studies demonstrate that both line-carried power and the longitudinal component of voltage drop positively correlate with voltage stability, enabling rational DG power regulation. Furthermore, on the hybrid dataset D, the GCN-BiLSTM-Attention model achieves an accuracy of 96.62% and an F1 score of 98.38%, indicating high predictive precision. This method enables precise delineation of system instability zones, facilitating emergency control operations in power systems.

Keywords: High-density distributed generation; Transparent grid; Graph convolutional network; Bidirectional long short-term memory network; Attention mechanism

1. Introduction

With the continuous depletion of fossil fuels and the worsening of environmental pollution, the energy and environmental crises have become shared challenges for the development of all human societies. Due to the convenience of electricity transmission and flexibility of use, distributed energy generation has emerged as the preferred form for developing and utilizing new energy sources. Its characteristics—cleanliness, renewability, and widespread distribution—have garnered extensive attention and application [1-3]. However, the large-scale integration of distributed power sources has profoundly impacted power grids.

The integration of distributed power sources has significantly altered the topology of power grids. Traditional radial grids are gradually transforming into complex networks incorporating multiple distributed nodes, increasing grid complexity and management difficulty [4-6]. Furthermore, the integration of distributed power sources presents new challenges for voltage control in power grids. Particularly in low-voltage distribution grids with extensive distributed photovoltaic (PV) integration, the output of PV generation is highly dependent on sunlight conditions. The resulting fluctuations in output power can cause frequent voltage variations in the grid [7-9]. For instance, during sunny weather, increased PV output may lead to excessive local grid voltage, while reduced output on cloudy days or at night may cause voltage dips. Simultaneously, the variability of distributed generation complicates frequency stability control. The unstable power output from distributed sources makes it difficult to

maintain active power balance in the grid, potentially causing frequency fluctuations. These fluctuations not only affect grid stability but may also damage users' electrical equipment [10-13]. Traditional grid voltage control methods suffer from response delays and insufficient prediction accuracy [14-15]. Under the “dual carbon” strategy, the exponential growth of distributed energy sources connecting to the grid by 2025 will correspondingly increase the frequency of voltage fluctuations. Consequently, monitoring and early warning of voltage stability have become critically important [16].

The transparent power grid represents a new developmental paradigm emerging from the integration of power grids with next-generation information and communication technologies, exemplified by the internet, within the context of the energy transition. By applying internet concepts and advanced technologies such as big data, cloud computing, IoT, mobile networks, artificial intelligence, and blockchain, it consolidates and innovates existing fragmented systems and platforms. This enhances perception and control capabilities across the entire “generation-grid-load-storage” chain, substantially improving the construction, operation, maintenance, and management standards of power grids [17-19]. Furthermore, it breaks down operational barriers in control and management, harnesses massive amounts of end-user and operational big data, and achieves transparent management of energy flows, business processes, and data streams. This enables optimal resource allocation and fosters a power-driven energy ecosystem [20-23]. However, the integration of distributed energy sources continues to challenge voltage stability in transparent grids, highlighting the urgent need for in-depth research into dynamic voltage stability monitoring and early warning technologies.

Widely applied voltage stability monitoring and early warning methods utilize sensitivity analysis, machine learning, and neural networks. Reference [24] integrates data from the Data Acquisition and Supervisory Control System (DAS/SCADA) and phasor measurement units (PMUs). By calculating voltage stability margins using indicators derived from the impedance matching theorem, it achieves voltage stability monitoring while locating voltage weak nodes to issue warnings during instability. Reference [25] employs machine learning for long-term voltage stability monitoring, using load capacity indicators as observation metrics. Relevant index data is input into machine learning models for training, incorporating diverse operational conditions and fault scenarios. System validation confirms this monitoring method possesses both accuracy and robustness. Reference [26] designed an online application algorithm combining a simplified two-generator-one-load model with voltage data. It achieves real-time short-term voltage stability monitoring through two modules: pre-fault analysis and real-time monitoring. Reference [27] employs a divergent deep neural network trained with limited labeled data to achieve novel voltage stability monitoring under time-varying conditions, maintaining a 95.48% monitoring accuracy during environmental transitions. Reference [28] addresses the continuous equipment updates required for monitoring and controlling grid voltage stability due to distributed energy resource integration by designing a distributed computing coordination platform that monitors and controls voltage stability using real-time data. Based on dynamic response and topological information visualization, [29] introduces sliding 3D convolutional neural networks to learn voltage spatiotemporal correlations. Its computational efficiency and versatility enable long-term, real-time, continuous voltage stability monitoring across diverse disturbance environments. Reference [30] divides the power system into zones and integrates phasor-based information to perform long-term voltage stability estimation under the Kernel Learning Machine (KLM) intelligent method. This approach enables voltage stability monitoring, predicts certain voltage instability scenarios, and issues voltage instability alerts during reactive power shortages. Reference [31] employs the Thevenin equivalent technique and synchronous phasor measurement units (SPMUs) to establish a real-time monitoring system for grid voltage stability during geomagnetic storms. This system relies on SPMUs to determine Thevenin equivalent parameters for implementation.

However, during application, it was discovered that methods based on traditional machine learning, deep neural networks, and convolutional neural networks struggle to effectively capture scenarios involving rapid fluctuations in distributed energy resources, as well as relevant information before and after voltage collapses [32-33]. Long Short-Term Memory (LSTM) networks, however, demonstrate significant advantages in handling long-term dependency issues and are thus employed for grid monitoring and early warning. Reference [34] employs a semi-supervised clustering algorithm to capture category labels in short-term voltage stability instances, using LSTM for real-time estimation of voltage stability under dynamic trajectories following disturbances. Reference [35] combines a time-series convolutional neural network with LSTM, utilizing post-disturbance bus voltage time-series trajectory models as input data to predict power system stability. Integrating transfer learning, it performs real-time assessment of short-term voltage stability based on network topology changes, thereby enabling voltage stability monitoring.

This paper first establishes a mathematical model for high-density distributed power sources. Leveraging massive, real-time, multi-source data obtained from transparent power grids, it constructs

multi-dimensional time-series inputs to quantitatively analyze the transient voltage stability of the system and individual nodes after integrating high-density distributed power sources into transparent grids. In model construction, a bidirectional long short-term memory (BiLSTM) neural network replaces the traditional long short-term memory (LSTM) network. By introducing an attention mechanism, the proposed BiLSTM-Attention model demonstrates enhanced capability in extracting critical features. Finally, to address the issue of insufficient grid information utilization, we integrate a Graph Convolutional Neural Network (GCN) into the BiLSTM-Attention model to extract spatial features from topological data. This results in the GCN-BiLSTM-Attention network fusion model, which further enhances the accuracy of grid voltage stability prediction. Relevant case studies are designed for validation and analysis.

2. Voltage Stability of Transparent Grids with High-Density Distributed Power Source Integration

2.1. Modeling Distributed Power Sources Connected to the Grid

2.1.1. Photovoltaic Array Modeling

Currently, distributed photovoltaic systems commonly consist of multiple basic photovoltaic units. Each basic photovoltaic unit can be regarded as a current source with internal resistance. In practical engineering applications, the equivalent circuit of a basic photovoltaic unit can be represented by Equations (1) and (2):

$$I = I_{SC}\left(1 - C_1(e)^{(V-CV)/C2VDC} - 1\right) + DI \tag{1}$$

$$\begin{cases} C_1 = \left(1 - I_m / I_{sc}\right) e^{-V_m / C_2 V_{DC}} \\ C_2 = \left(V_m / V_{oc} - 1\right) / \ln\left(1 - I_m / I_{sc}\right) \\ DI = \alpha R / R_{ref} DT + \left(R / R_{ref} - 1\right) I_{sc} \\ DV = -\beta DT - R_s DT \\ DT = T - T_{ref} \end{cases} \tag{2}$$

In the equation: I_{sc} denotes the short-circuit current; V_{oc} denotes the open-circuit voltage; R, R_{ref} denote solar radiation and radiation reference values; T, T_{ref} denote cell temperature and reference temperature; α denotes the temperature coefficient of current variation; β denotes the temperature coefficient of voltage variation; R_s is the series resistance of the photovoltaic array.

Currently, the most commonly used maximum power point tracking (MPPT) methods for photovoltaic power generation systems include fixed voltage method, fuzzy control method, intermittent scanning method, and disturbance observation method.

2.1.2. Fan Modeling

Wind turbines convert wind energy into mechanical energy. Based on aerodynamic principles, the output power of a wind turbine is primarily related to wind speed, rotor area, and the coefficient of wind energy utilization, and can be expressed as:

$$P_{out} = \frac{1}{2}\rho\pi R^2 V^3 C_P(\lambda, \beta) \tag{3}$$

In the equation: P_{out} represents the output power of the wind turbine; ρ denotes the air density; R indicates the rotor radius; V signifies the wind speed; C_p is the power coefficient, which is a nonlinear function of the tip speed ratio λ and the pitch angle β. Wind turbines are primarily categorized into doubly-fed wind generators and permanent magnet wind generators, with the former being predominantly used in distributed wind turbines.

2.1.3. Battery Modeling

The modeling employs the Shepard battery model, which simplifies the battery into a controlled voltage source with internal resistance. The mathematical model of this battery can be expressed as:

$$V_b = V_o - K\frac{Q}{Q - \int I_b \mathrm{d}t} + Ae^{(-B/I_b dt)} \tag{4}$$

In the equation: V_b is the open-circuit voltage of the battery, V_o is the output voltage of the battery; K is the polarization voltage; Q is the battery capacity, $\mathrm{A}\cdot\mathrm{h}$; A is the exponential gain voltage; B is the time gain capacity, $\mathrm{A}\cdot\mathrm{h}^{-1}$.

2.1.4. Modeling of Micro Gas Turbines

The primary components of a micro gas turbine include the micro gas turbine itself, a permanent magnet generator, power electronics, and corresponding control modules. A simplified mathematical model of the micro gas turbine can be represented as:

$$f_1 = T_{ref} - 700\left(1 - u_1\right) + 550(1 - \omega) \tag{5}$$

$$f_2 = 1.3\left(u_2 - 0.23\right) + 0.5(1 - \omega) \tag{6}$$

In the equation: f_1 is the exhaust port temperature function; f_2 is the turbine torque output function; T_{ref} is the temperature reference value, typically set to 950; u_1 is the exhaust port temperature; ω denotes the generator rotational speed; u_2 is the turbine fuel capacity.

2.2. Key Technologies for Transparent Power Grids

The transparent power grid technology system primarily encompasses key technologies across the perception layer, network layer, platform layer, and application layer. The overall framework of the transparent power grid technology system is illustrated in Figure 1, as detailed below.

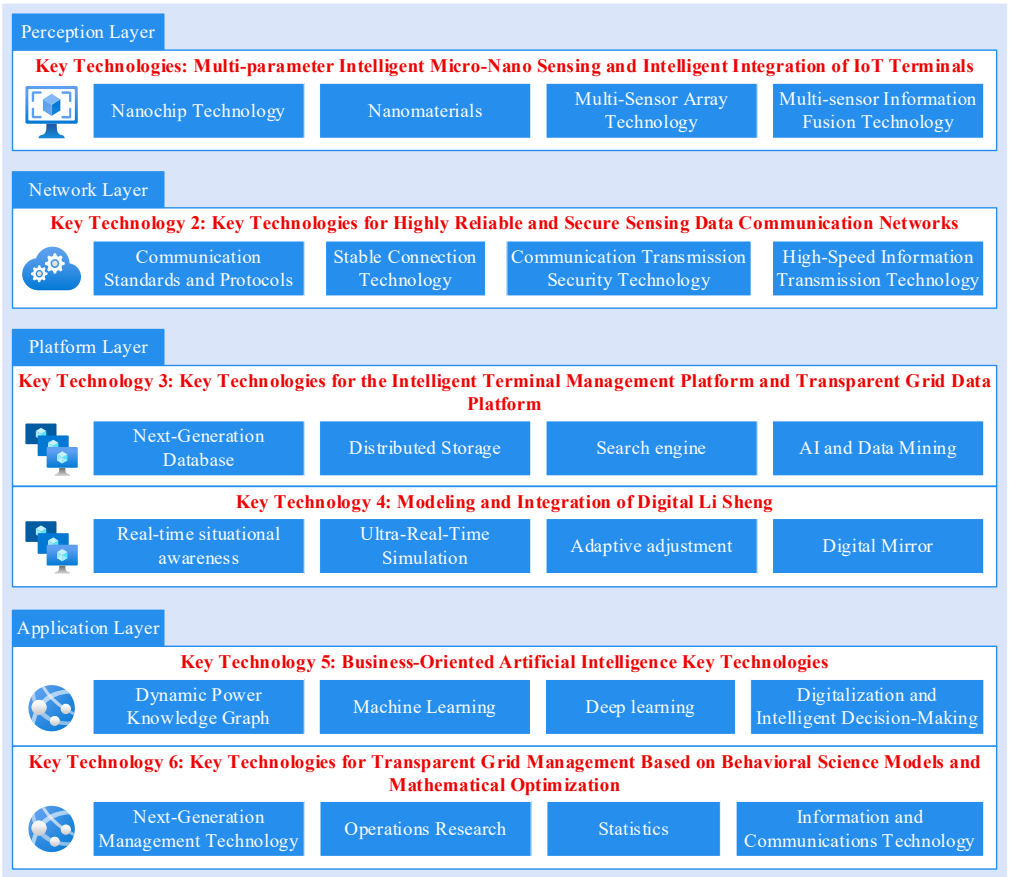

Figure 1. The overall framework of the transparent grid technology system.

2.2.1. Key Technologies at the Perception Layer

The perception layer aims to provide information collection services for the construction and operation of transparent power grids, with the key focus on building an intelligent integrated system of IoT terminals composed of multi-parameter smart micro-nano sensors. By integrating multi-parameter sensors with multi-channel technologies, it enables multi-parameter data collection to enhance information transparency and reliability, increase information value, extend sensing cycles, and reduce deployment and maintenance costs. Intelligent micro-nano sensors leverage sub-nanometer process chips and nanomaterial technologies to reduce sensor size, thereby increasing application versatility and spatial efficiency. This enhances the self-maintenance and self-learning capabilities of sensing terminals, enabling them to participate in intelligent feedback and auxiliary decision-making.

2.2.2. Key Technologies at the Network Layer

Breakthroughs in technologies such as extensive deployment and stable connectivity of network infrastructure, secure communication transmission, and high-speed information transfer, meeting the requirements of wide coverage, high reliability, and low latency for communication networks. Integrate key technologies spanning network planning, design, and maintenance—including communication standards and protocols, cybersecurity protection, and data transmission assurance—to build sensor data communication networks. Ensure both the volume and quality of data access, safeguard data privacy and security, and enhance the scope and efficiency of information utilization to elevate data application value. Mitigate potential risks during information transmission and minimize data loss.

2.2.3. Key Technologies at the Platform Layer

First, key technologies for the intelligent terminal management platform and transparent power grid platform. Intelligent terminals provide sensing capabilities aimed at delivering target information to support decision-making, thereby requiring oversight from the transparent power grid. The intelligent management platform accounts for constraints such as terminal operating environments and real-time grid demands, utilizing technologies like AI to manage the operational status of massive numbers of intelligent terminals. These terminals serve as interfaces for vast amounts of multi-source, heterogeneous data, with the resulting big data constituting a critical asset for the transparent power grid. Employing next-generation databases, distributed storage, and other technologies, it efficiently organizes, stores, and processes data. Utilizing search engines and related technologies, it rapidly retrieves required data to accelerate subsequent development processes. Additionally, the data platform spawns applications such as data analysis and data mining, not only supporting transparent grid operations but also providing feedback across the entire data collection and processing workflow.

Second, key technologies for digital twin modeling and integration. Digital twin models originate from compressed representations of real physical systems, selecting prominent features to reconstruct corresponding digital models. Research should focus on developing feature compression methods tailored to the characteristics of each transparent grid component, selecting optimal approaches to construct virtual models. Digital twins fully leverage real-time and historical data resources to achieve virtual-physical synchronization between digital models and physical systems. Through processes like real-time situational awareness and ultra-real-time simulation, dynamic virtual digital models are constructed. Establishing a digital twin platform creates a disassemblable, transferable, modifiable, and repeatable digital mirror. This assists operators in gaining deep insights into physical grid entities, enabling current state assessments, historical diagnostics, and future predictions. Comprehensive decision-making is supported through thorough simulation of various possibilities.

2.2.4. Key Application Layer Technologies

First, business-oriented AI core technologies. Addressing the intelligent rapid response requirements of transparent power grid operations, business-oriented AI core technologies—specifically the integration of dynamic power knowledge graphs with AI—possess systematic problem-solving capabilities. Represented by machine learning and deep learning, AI technologies perform data representation learning, deeply mining and interpreting dynamic power knowledge graphs. By selecting information relationships as entry points, they fully achieve the integration, analysis, and judgment of knowledge features.

Second, key management technologies for transparent grids based on behavioral science and mathematical optimization. Leveraging behavioral science theories and mathematical optimization principles, data-driven mathematical management models are established to pursue efficient management and create management value. Multi-parameter micro-sensors within the transparent grid's perception

layer provide foundational conditions for grid data collection, further expanding the application scenarios of traditional sensors.

2.3. Analysis of the Impact of Distributed Power Source Integration on System Stability

2.3.1. Selection of Stability Indicators

(1) Frequency Stability: Frequency stability measures a power system's ability to maintain grid frequency stability during load changes or other disturbances. Excessive frequency fluctuations may cause equipment damage or system collapse. In simulations, we will record grid frequency changes before and after DG output fluctuations and set frequency deviation alert thresholds (e.g., ±0.1 Hz).

(2) Voltage Stability: Voltage stability focuses on whether the system can maintain node voltages within permissible ranges after DG integration. Voltage deviations may cause abnormal operation or damage to electrical equipment. We will monitor voltage level changes at nodes near DG connection points and set voltage deviation limits (e.g., ±5% of rated voltage).

(3) Phase Angle Stability: Phase angle stability involves changes in the relative rotor angles between synchronous generators. While most DGs do not directly participate in synchronization, their behavior can impact system phase angle stability under certain conditions—such as when large-scale wind farms or photovoltaic power plants connect to the AC grid via inverters. We will analyze changes in the maximum phase angle difference between synchronous generators before and after DG integration and establish a critical threshold (e.g., ±30°).

2.3.2. Mathematical Modeling

Based on the selected stability indicators above, construct a dynamic model of the power system incorporating DG. This model should include the following components:

Power System Model: First, establish a mathematical model of the conventional power system, covering the dynamic behavior of components such as generators, transformers, and transmission lines, as well as load characteristics. For example, a synchronous generator can be represented by a classical fourth-order model, which includes four state variables: rotor angular velocity, rotor angle, excitation current, and electromagnetic torque.

Distributed Generation Model: Subsequently, integrate the DG model. Taking a photovoltaic power generation system as an example, its output power PPV can be expressed as:

$$P_{PV} = A \cdot I_{solar} \cdot \eta_{eff} \tag{7}$$

Where A represents the photovoltaic panel area, I_{solar} denotes the incident solar radiation intensity, and η_{eff} indicates the conversion efficiency.

Interaction Model: Finally, establish an interaction model between DG and the main grid. For example, the impact of inverter control strategies (such as PQ control, VF control) on system frequency and voltage can be described by the following equations:

$$V = \frac{P + jQ}{I} \tag{8}$$

Here, V denotes the inverter output voltage, P and Q represent active power and reactive power respectively, and I is the current.

3. Grid Voltage Stability Assessment Based on Long Short-Term Memory Networks

3.1. DG Grid Connection Voltage Stability Prediction Model Architecture

3.1.1. Long Short-Term Memory Neural Networks

(1) Forgetting gates

The role of the forgetting gate f_t is to learn the appropriate proportion of forgetting for the network, to reduce the impact of too much memory on the present input of the neural network, and to selectively retain or forget which information. Specifically, the input x_t of the model at the moment t and the output h_{t-1} of the hidden layer at the moment $t-1$ are linearly transformed, and the activation function sigmoid is applied to obtain the output value. The σ function compresses any output onto (0,1), controlling the memorization and forgetting of different information. It is calculated as in equation (9):

$$f_t = \sigma\left(W_f x_t + U_f h_{t-1} + b_f\right) \tag{9}$$

Here, σ is the activation function that sets the information flow weight. x_t is the input vector at time t, h_{t-1} is the hidden state information at time $t-1$, and b_f, W_f and U_f represent the biases, input weights, and recurrent weights of the forget gate, respectively.

(2) Input Gate

After information is discarded via the forget gate, the input gate determines which information is stored in the cell state. First, it extracts relevant information C_t from the current input. Then, it uses the sigmoid function to control how much of this memory enters the cell state, deciding which information i_t to add. After obtaining f_t and i_t at the current time step, the candidate state of the previous time step node is updated from $C_{t-1} \to C_t$, as described in Equations (10) to (12):

$$C_t = \tanh\left(W_c x_t + U_c h_{t-1} + b_c\right) \tag{10}$$

$$i_t = \sigma\left(W_i x_t + U_i h_{t-1} + b_i\right) \tag{11}$$

$$C_t = C_{t-1} \cdot f_t + C_t \cdot i_t \tag{12}$$

Among these, i_t represents information retained through the Sigmoid function, C_t denotes newly added input information, σ and tanh serve as activation functions, C_{t-1} corresponds to the internal state at time $t-1$, and C_t indicates the internal state at time t.

(3) Output Gate

The output gate determines the hidden state output h_t at the current time step based on the current input x_t, the previous hidden state output h_{t-1}, and the candidate state C_t of the current node. This completes the model's extraction of historical information. The calculation method is shown in Equations (13) to (14):

$$o_t = \sigma\left(W_o x_t + U_o h_{t-1} + b_o\right) \tag{13}$$

$$h_t = o_t \cdot \tanh\left(C_t\right) \tag{14}$$

In the original LSTM model, the model can only learn data features from past time steps. However, the vast majority of predictions require input from both preceding and subsequent time steps to enhance prediction accuracy. The bidirectional long short-term memory network (BiLSTM) connects two LSTMs in opposite directions, constructing forward and backward propagation hidden layers to enable bidirectional data flow from past and future time steps [36]. Thus, in the BiLSTM model, the grid features at the current time step simultaneously utilize information from both forward and backward directions. The outputs from the two LSTMs are concatenated to complete the task of better extracting the correlation features in the time-series data.

The model's calculation formulae are shown in (15) and (16):

$$h_t = LSTM\left(x_t, h_{t-1}\right) \tag{15}$$

$$h_t = LSTM\left(x_t, h_{t-1}\right) \tag{16}$$

Here, h_t denotes the hidden layer state during forward propagation at time t, h_t denotes the hidden layer state during backward propagation at time t, LSTM represents the LSTM neural unit, and x_t denotes the input at time t. By combining the two hidden layer components h_t and h_t, the output H_t is formed.

3.1.2. Attention Mechanism

The computational principle of the attention mechanism is as follows: First, the attention layer calculates the similarity S_{ti} tth hidden state in the encoder and each hidden state of the encoder. A higher score indicates greater attention and a larger weight. Next, the similarity coefficients undergo softmax normalization to yield the normalized attention vector α_{ti}; Based on this, the product F is computed between the hidden layer state and the attention weights α_{ti}; The network ultimately

produces the output h_t' from the attention layer, weighted with varying importance. The specific calculation method is shown in Equations (17) to (20):

$$S_{ti} = V \tanh\left(Wh_t + Uh_i + b\right), i = 1,2,3,t-1 \tag{17}$$

$$\alpha_{ti} = \frac{\exp\left(S_{ti}\right)}{\sum_{k=i}^{t} \exp\left(S_{tk}\right)}, i = 1,2,3,t-1 \tag{18}$$

$$F = \sum_{i=1}^{t} \alpha_{it} \times h_i, i = 1,2,3,t-1 \tag{19}$$

$$h_t' = Attention\left(F, h_t, x_t\right) \tag{20}$$

Here, x_1, x_2, x_3, x_t denotes the input sequence, h_1, h_2, h_3, h_t are the hidden layer state values of the input sequence x_1, x_2, x_3, x_t, and W, V, U, b are the parameters that the model needs to learn and continuously update during training.

3.1.3. BiLSTM-Attention Voltage Prediction Model Architecture

This chapter addresses the challenge of feature extraction in the temporal dimension of power grid voltage data by employing a BiLSTM-based attention mechanism for grid voltage stability prediction. Its core concept involves introducing an attention mechanism into the output of each time step in the BiLSTM network to calculate the similarity between the current time step and historical time steps. This yields normalized weights from the attention layer, which are then multiplied by the BiLSTM output and summed to produce the BiLSTM-attention output. This approach enables the model to learn voltage features bidirectionally across the time dimension while incorporating valuable information through the attention module. The architecture of the BiLSTM-attention grid voltage stability prediction model is illustrated in Figure 2, comprising four main components:

(1) Input Layer: Inputs preprocessed and feature-selected grid voltage data, with the number of input nodes set to the feature count of the voltage data.

(2) BiLSTM Layer: The primary function of the BiLSTM layer is to extract bidirectional temporal information from the grid voltage data. Specifically, the built-in bidirectional propagation parameter in the LSTM model from torch.nn is set to True, and the number of hidden layer neurons (n_hidden) is set to 64. resulting in 128 hidden layer output units after concatenating the forward and backward LSTM networks. Thus, the BiLSTM model's output bilstm_output has shape (time_steps, input_shape, 2*n_hidden). The shape of the hidden layer's output values hn is (2, time_steps, n_hidden), where input_shape represents the number of input nodes and time_steps denotes the time step length.

(3) Attention Layer: In the attention layer, the normalized weights are obtained by calculating the similarity between the current time step and previous time steps. These weights are multiplied with the BiLSTM output and summed to produce the BiLSTM-attention output, where the normalization function is softmax().

(4) Fully Connected Layer: Within the fully connected layer, the Linear() function from torch.nn performs dimensionality transformation on the updated feature vectors. The transformed dimension corresponds to the number of days being predicted.

3.2. Image Convolutional Neural Networks

Each graph convolutional network layer of the GCN network can be expressed as a nonlinear function as shown in equation (21). Since the development of the network, researchers have improved the function f three times, which are shown in Eqs. (22)~(24), where $\sigma(\cdot)$ is the activation function (usually ReLU) for all layers except the output layer, A is the adjacency matrix, and $A = A + I$ denotes the adjacency matrix after the addition of the self-connection, and $D^{-\frac{1}{2}}$ represents the degree matrix after the introduction of the regularization trick, which can be directly calculated by the computer based on the input adjacency matrix in the operation. $W^l \in R^{N \times D}$ represents the output of the l th layer of the graph convolution, when l is equal to 0, $H^0 = X$ is the feature matrix of the data, W^l denotes the learnable parameter of the l th layer, and L is the Laplace matrix, $L = D - A$.

$$H^{l+1} = f\left(H^l, A\right) \tag{21}$$

$$H^{l+1} = \sigma\left(AH^{l}W^{l}\right) \tag{22}$$

$$H^{(l+1)} = \sigma\left(LH^{l}W^{l}\right) \tag{23}$$

$$H^{(l+1)} = \sigma\left(D^{\frac{1}{2}}AD^{\frac{1}{2}}H^{l}W^{l}\right) \tag{24}$$

In order to effectively extract the spatial feature information of transient voltage, this section adopts the implementation based on the convolution of spectral domain map for transient voltage stability assessment model construction, whose core principle is shown as follows.

First, the spatial feature information of the power system topological map is described by the normalized Laplace matrix in the frequency domain:

$$L_m = I - D^{-1/2}AD^{-1/2} \tag{25}$$

where L_m represents the normalized Laplace matrix; I represents the unit matrix; A represents the adjacency matrix of the power system topology graph; and D represents the diagonal matrix of the corresponding node degree of A. Where the elements in D are obtained by computing the elements in A, which can be expressed as:

$$D_{ii} = \sum_{j=1}^{j=n}\left(A_{ij}\right) \tag{26}$$

Then, perform spectral decomposition on L_m to extract the spatial feature information of the power system topology:

$$L_m = U\Delta U^{T} \tag{27}$$

In the formula, Δ represents the diagonal matrix composed of the eigenvalues of L_m; U represents the matrix of eigenvectors sorted according to the eigenvalues of L_m.

Simultaneously, by analogy with the traditional convolution formula, a graph convolution formula applicable to power system topology graphs can be derived:

$$x * Gg = U\left(U^{T}xU^{T}g\right) \tag{28}$$

In the equation, G represents the power system topology graph requiring graph convolution operations; x denotes the eigenvectors of the power system topology graph; g represents the convolution kernel; * denotes graph convolution; and denotes the Hadamard product.

Furthermore, define $g_\theta = diag\left(U^{T}g\right)$ as a learnable convolution kernel, thereby obtaining the spectral-based graph convolution formula:

$$x * Gg = Ug_\theta U^{T}x \tag{29}$$

Finally, to reduce computational complexity and improve processing speed, Chebyshev polynomials are employed to approximate the convolution kernel:

$$\Delta_Z = 2\Delta / \lambda_{\max} - I \tag{30}$$

$$g_\theta = g_\theta(\Delta) = \sum_{i=0}^{K}\theta_i T_i\left(\Delta_Z\right) \tag{31}$$

In the equation, Δ_Z represents the scaled eigenvector matrix; $\lambda_{\max}$ denotes the maximum eigenvalue of L_m; $T_i()$ denotes the i th-order Chebyshev polynomial; θ_i denotes the corresponding Chebyshev coefficient; K denotes the number of Chebyshev polynomial terms. Where, $T_i\left(\Delta_Z\right) = 2\Delta_Z T_{i-1}\left(\Delta_Z\right) - T_{i-2}\left(\Delta_Z\right); T_0\left(\Delta_Z\right) = 1; T_1\left(\Delta_Z\right) = \Delta_Z$.

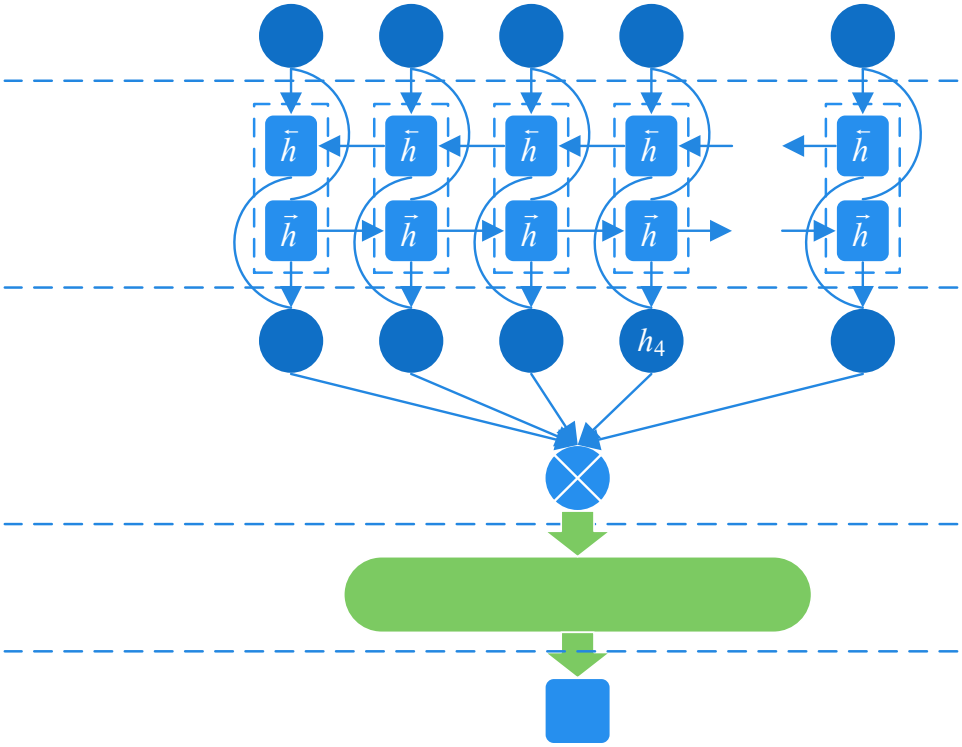

Figure 2. The BiLSTM-attention model structure.

3.3. Voltage Stability Assessment Based on GCN-BiLSTM-Attention

3.3.1. Design of Transient Voltage Stability Assessment Model

To enhance the accuracy of transient voltage stability assessment, it is necessary to comprehensively consider the spatiotemporal distribution characteristics of transient voltages. Input features for the transient voltage stability assessment model should be constructed from both temporal and spatial perspectives. Regarding the temporal characteristics of transient voltages, since transient voltage stability depends on multiple factors beyond voltage alone—such as: during power system transients, changes in voltage magnitude and phase angle directly reflect the system's transient voltage response characteristics and are closely related to transient voltage stability; Active power and reactive power represent power flow and consumption within the system. Their changing trends may cause voltage fluctuations, thereby triggering transient voltage instability risks. Therefore, node voltage magnitude and phase angle time series data U_t, θ_t along with active power and reactive power time series data P_t, Q_t are adopted as input features. Regarding spatial features of transient voltage, to account for the influence of power system topology on energy transmission paths and distribution patterns, and to consider dynamic interactions between nodes in order to capture the spatial evolution of transient voltage, the system topology structure A is adopted as an input feature.

The input features for the transient voltage stability assessment model are as follows:

$$U_t = \begin{pmatrix} u_1 & u_2 & \cdots & u_L \end{pmatrix} \tag{32}$$

$$\theta_t = \begin{pmatrix} \theta_1 & \theta_2 & \cdots & \theta_L \end{pmatrix} \tag{33}$$

$$P_t = \begin{pmatrix} p_1 & p_2 & \cdots & p_L \end{pmatrix} \tag{34}$$

$$Q_t = \begin{pmatrix} q_1 & q_2 & \cdots & q_L \end{pmatrix} \tag{35}$$

$$A = \begin{pmatrix} a_{11} & a_{12} & \cdots & a_{1n} \\ a_{21} & a_{22} & \cdots & a_{2n} \\ \cdots & \cdots & \cdots & \cdots \\ a_{n1} & a_{n2} & \cdots & a_{nn} \end{pmatrix} \tag{36}$$

In the formula, t represents the sampling interval of the input feature; L denotes the sampling window length of the input feature; n indicates the number of nodes in the evaluation region; the elements in A represent the connection relationships between nodes within the evaluation region, where 1 and 0 signify connected and disconnected nodes, respectively.

Furthermore, the sampling time interval of the transient voltage stabilization evaluation model's input features is denoted as t_d. The number of data points collectable per t_d is represented as α. The sampling interval t is expressed as $\left[t_c - t_d, t_f + \lambda t_d\right]$ is defined. The sampling window length $L = \alpha\left[\lambda t_d + \left(t_f - t_c\right) + t_d\right] / t_d = \beta + \mu + \eta$ is defined. Here, β represents the number of sampling points during steady-state operation; μ represents the number of sampling points during the fault period; and η represents the number of sampling points after fault clearance.

The output of the transient voltage stability assessment model is fundamentally the classification result of a multi-binary classification task, corresponding to the transient voltage stability status of each node in the assessment area, where 0 and 1 represent transient voltage stability and instability, respectively. The criteria for transient voltage stability determination are as follows: During the transient process after a fault, the voltage at the system's central busbar must not remain below 0.75 pu for more than 1 second. Furthermore, after the transient process concludes, the voltage at the central busbar for voltage levels of 220 kV and above must not fall below 0.9 pu.

3.3.2. Transient Voltage Stability Dynamic Monitoring and Early Warning Process

The transient voltage stability assessment process based on GCN-BiLSTM is illustrated in Figure 3, comprising two phases: offline training and online evaluation. The specific steps for the offline training phase are outlined as follows: 1) - 6).

1) Simulation Data Generation: Generate extensive simulation data using the PSD-BPA time-domain simulation software. Enhance the richness and diversity of sample data by varying power flow levels, fault locations, and load compositions.

2) Voltage Stability State Determination: Based on power system transient voltage stability criteria and simulation data, determine the transient voltage stability state at each node.

3) Input Feature Selection: Select input features for the transient voltage stability assessment model from the generated simulation data, thereby constructing the sample sets required for model training, validation, and testing.

4) Model Training: Forward-train the transient voltage stability assessment model using the training set. Optimize model parameters based on backpropagation results to progressively reduce the error between model predictions and actual outcomes.

5) Model Validation: Perform forward propagation of the transient voltage stability assessment model using the validation set. Adjust model hyperparameters based on validation results to enhance the model's generalization capability.

6) Model Testing: Input the test set into the trained transient voltage stability assessment model for evaluation, and comprehensively assess the model's performance based on the test results.

Additionally, to achieve real-time monitoring of voltage states at each node within the transient voltage stability assessment area, the online assessment phase follows these steps: First, utilize PMU measurement devices to obtain real-time measurement data for the transient voltage stability assessment input features within the evaluation area. Then, employ the transient voltage stability assessment model trained during the offline training phase to determine the transient voltage stability status of each node in the evaluation area. Finally, based on the transient voltage stability assessment results, decide whether to implement control measures: if transient voltage stability is maintained, continue monitoring; otherwise, implement corresponding emergency measures.

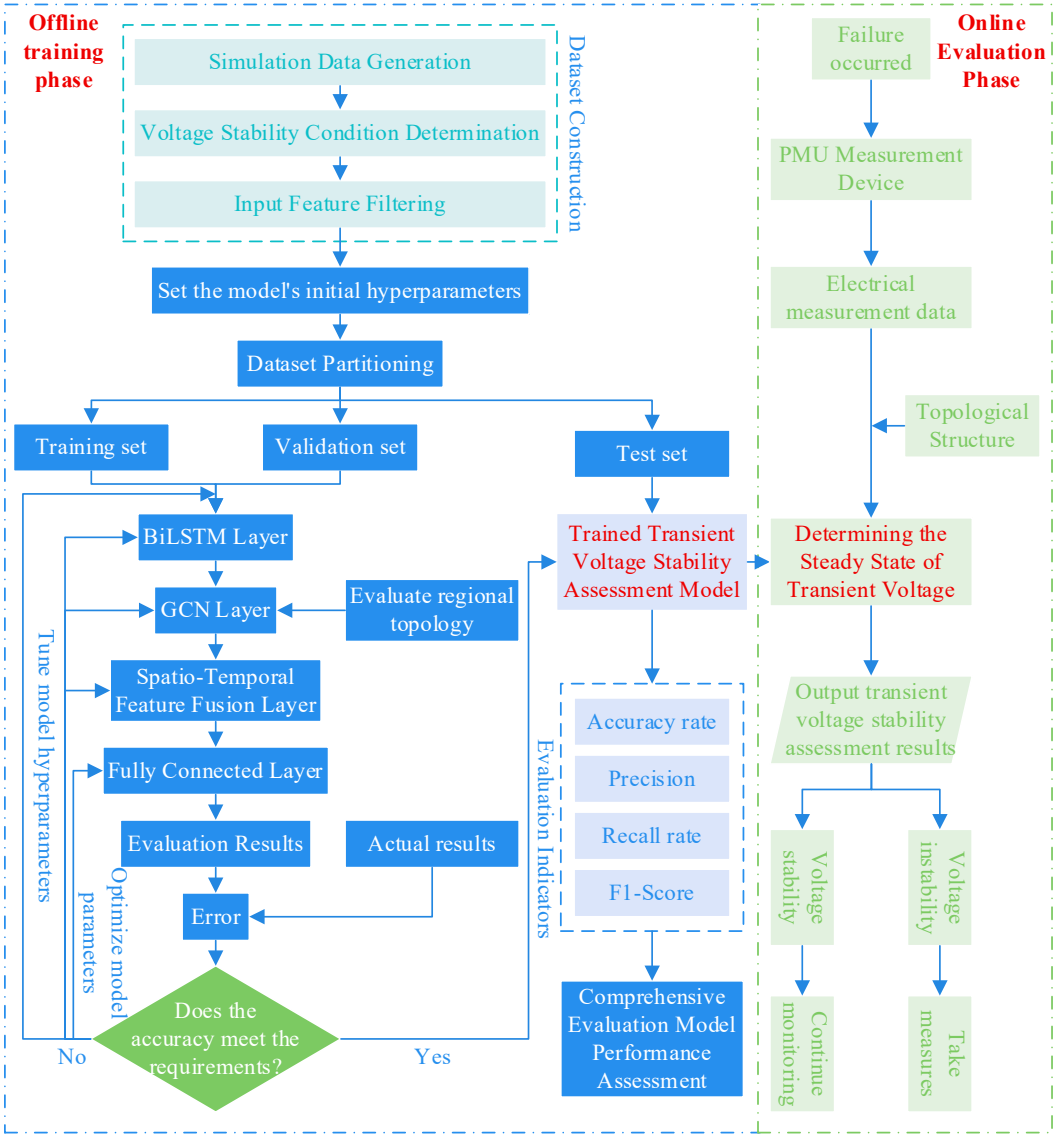

Figure 3. Transient voltage stability evaluation process.

4. Case Study Analysis

4.1. Analysis of the Impact of High-Density DG Access on System Stability

Taking an IEEE 33-node distribution network system as an example, this study analyzes the impact of distributed power sources on voltage stability in distribution networks. The original system is illustrated in Figure 4, with its voltage stability L-index and H-index shown in Figure 5.

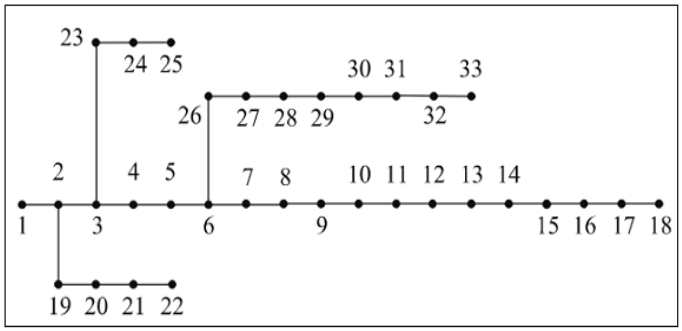

Figure 4. IEEE 33node distribution network.

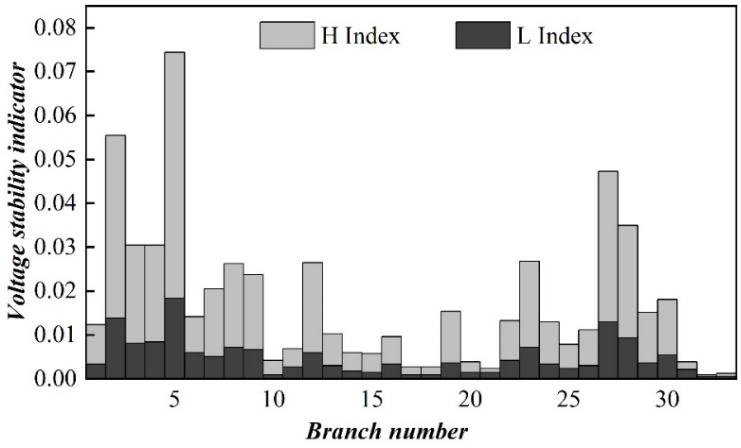

Figure 5. IEEE 33node system voltage stability index.

A distributed generation (DG) unit with a capacity of 1.5 MV·A is connected at node 33. Calculate the voltage stability H index for each branch of the system under different high-density DG power factors, as shown in Figure 6.

With a load of 0.65 + j0.45 MVA connected at node 33, the power flowing through branch 32 (line 32-33) gradually decreases as the DG power factor increases, causing H to decrease. When both the power flowing through branch 32 and the horizontal component of voltage drop are small, H reaches its lowest point in branch 32. Additionally, the H values of other branches exhibit a positive correlation with the power flowing through the line and the voltage drop.

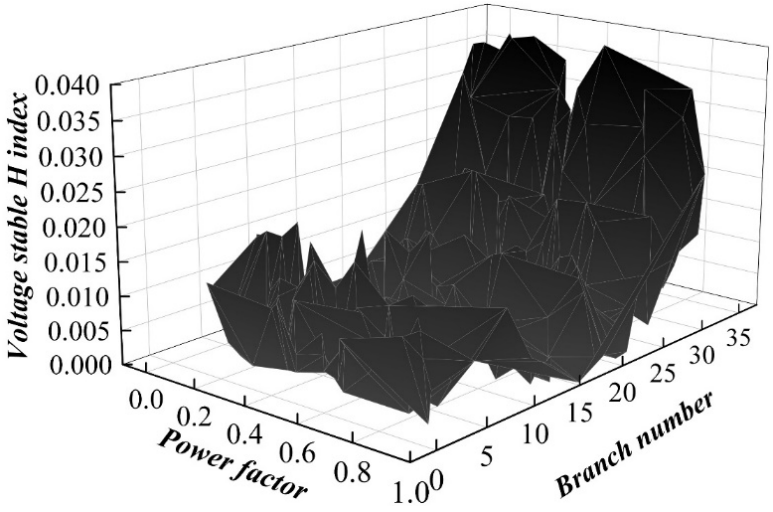

Figure 6. Voltage stability H index of each node under Different DG power factors.

The voltage stability L index for each branch of the system is shown in Figure 7. Figure 7 also reveals that the L value of Branch 32 first decreases and then increases as the high-density DG power factor rises. Changes in the high-density DG power factor at Node 33 alter the power flowing through other branches and the horizontal component of voltage drop. Based on the above analysis, it is evident that system voltage stability is significantly influenced by both the power flowing through each branch and the horizontal component of voltage drop: the smaller the power flowing through a line, the better the voltage stability. When line power flow is constrained, rationally adjusting DG power factor can effectively enhance system voltage stability. This analysis demonstrates that reducing branch power flow improves voltage stability within that branch. By rationally adjusting DG power factor to minimize the transverse voltage drop component, system voltage stability can be effectively enhanced.

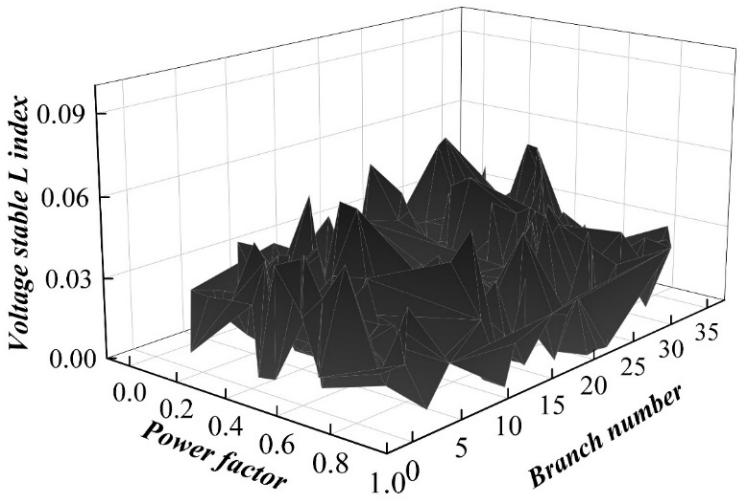

Figure 7. Voltage stability L index of each node under Different DG power factors.

4.2. Experimental Preparation

4.2.1. Dataset Partitioning

The original dataset comprises 7,800 samples, with 4,800 stable samples and 3,000 unstable samples. Based on topological categories, these can be divided into three sample sets: fully connected, N-1 broken connections, and N-2 broken connections. To facilitate verification of the model's adaptability to topological changes, the original samples were reorganized as shown in Table 1. Here, Dataset A represents the fully connected sample set, Dataset B represents the N-1 disconnected sample set, and Dataset C represents the N-2 disconnected sample set. A portion of samples was stratified from Datasets A, B, and C, maintaining consistency with the original sample set's category proportions, to form a mixed dataset D according to a specific ratio.

Table 1. Stable and Unstable samples of four data sets.

Data set	Stable	Unstable	Total
A	**2454**	**1244**	**3698**
B	**1550**	**950**	**2500**
C	**850**	**752**	**1602**
D	**1250**	**760**	**2010**

4.2.2. Selection of Evaluation Indicators

For transient stability assessment of power systems, our primary concern is whether the system loses stability after experiencing a large disturbance, meaning higher accuracy is required for predicting unstable samples. This paper selects accuracy P_{Acc}, precision P_{rec}, recall R_{ec}, and F_1 to evaluate model performance. However, achieving high recall by increasing the number of samples predicted as unstable is not feasible, as the probability of system recovery after transient processes is typically far greater than the probability of instability under normal conditions. Therefore, to address the trade-off between precision and recall, the F_1 metric is introduced to balance their respective impacts, providing a comprehensive evaluation of the classification performance for transient stability assessment classifiers.

4.3. Experimental Results and Analysis

4.3.1. Comparative Analysis of Model Performance

To validate the effectiveness of the proposed transient stability assessment model based on GCN-BiLSTM-Attention, without considering noise and data missing interference, corresponding transient stability assessment models were constructed using the networks composing the GCN-BiLSTM-Attention model. Performance comparisons were conducted on datasets with different topological structures, including GCN, SA-GCN, LSTM, TA-LSTM, and GCN-LSTM. Both GCN and SA-GCN are

two-layer classification models with input, hidden, and output dimensions consistent with the graph convolutional layer in the GCN-BiLSTM-Attention model. Due to the time-consuming nature of graph network training, the learning rate was increased to 0.01 to enhance training efficiency. LSTM and TA-LSTM also employ a two-layer model structure, with input-hidden and output dimensions consistent with the LSTM layer in the model. A dropout layer was added to prevent overfitting, with a dropout rate of 0.2 and a learning rate set to 0.001. The GCN-LSTM model structure and parameter settings align with the model. All models output transient stability assessment results via the Softmax function. The performance of different methods on the datasets is shown in Figure 8. (a) to (d) represent performance on Datasets A to D, respectively.

Figure (a) indicates that using GCN alone yields poor performance metrics for transient stability assessment, as graph network algorithms are unsuitable for feature extraction from time-series data. After employing the combined GCN-LSTM model, the evaluation accuracy improved from 89.44% to 96.72%. Precision and recall also improved, indicating that LSTM effectively extracted transient characteristics from the temporal features. The GCN-BiLSTM-Attention model achieved the best performance after incorporating the spatio-temporal dual attention mechanism, demonstrating not only the highest accuracy but also the optimal recall value, indicating a low misclassification rate for unstable samples.

Comparing Figures (c) with (a) and (b), the proposed GCN-BiLSTM-Attention model still exhibits the best performance metrics in comparative experiments on both the B and C line-break datasets. Its accuracy, recall, and F1 score are all the highest. Concurrently, it is evident that the GCN-BiLSTM-Attention model performs poorly on the N-2 open-circuit dataset C. This is attributed to significant variations in system topology, creating discrepancies between actual and complete topological connections. Consequently, the GCN-BiLSTM-Attention model fails to establish a comprehensive association between topological structures and node features, indicating low integration between spatial and temporal features. Therefore, further model validation is conducted using the hybrid dataset D.

Figure (d) shows that the performance of GCN-BiLSTM-Attention on hybrid dataset D is comparable to that on fully connected dataset A, achieving an accuracy of 96.62%. The F1 score of 98.38% indicates a favorable balance between precision and recall. This demonstrates that learning from fully connected samples enables the GCN-BiLSTM-Attention model to establish a comprehensive coupling between topological structure features (spatial features) and node collection features (temporal features). When classifying input samples under a disconnected topology, it achieves high evaluation accuracy, high recall, and high precision for unstable samples, delivering strong overall performance.

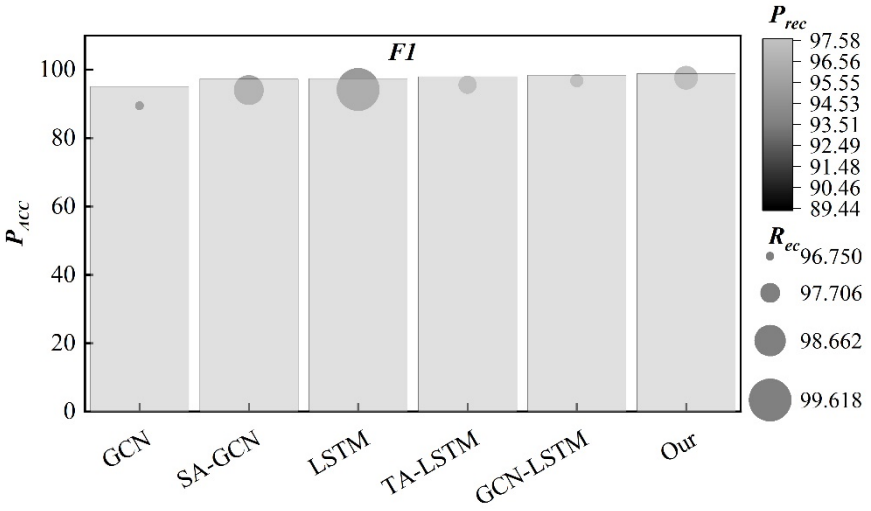

(a) Data set A

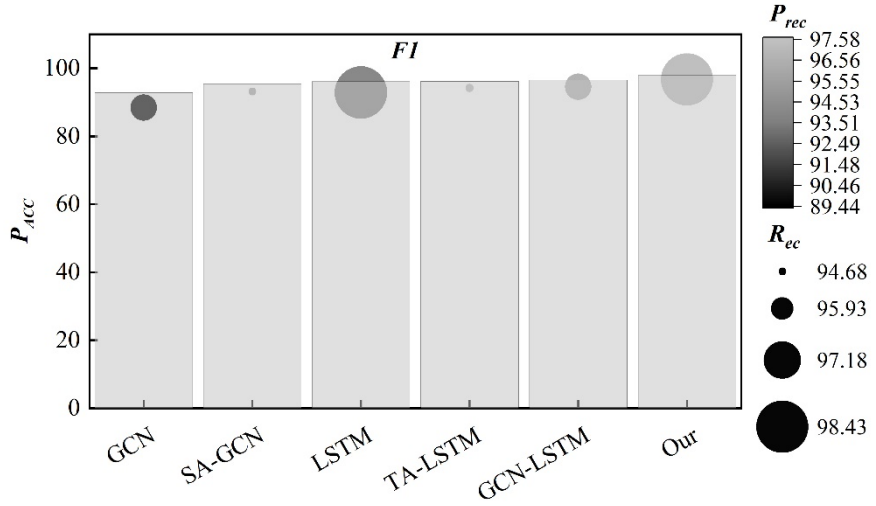

(b) Data set B

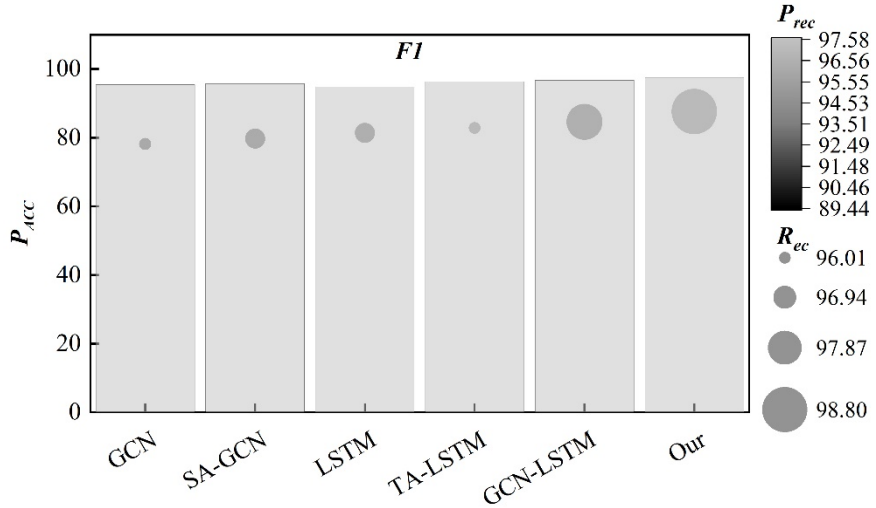

(c) Data set C

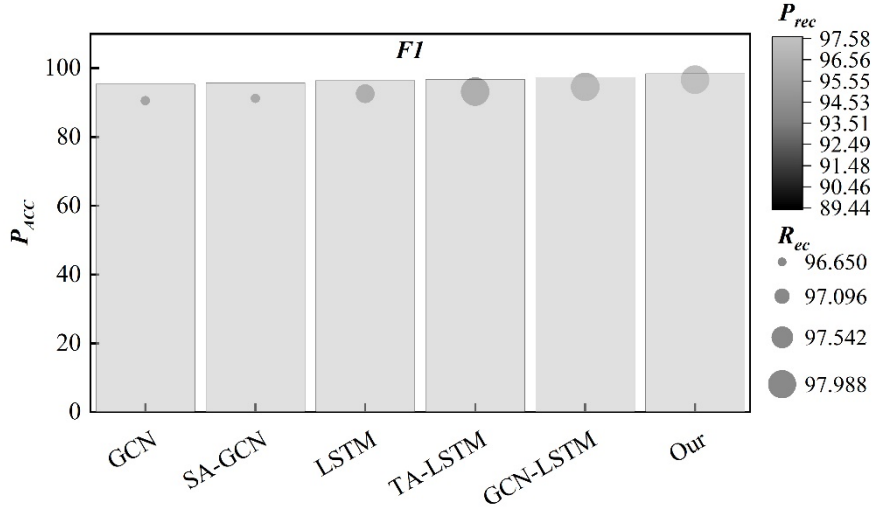

(d) Data set D

Figure 8. The performance of different method models in the data set.

4.3.2. Visualization of Model Feature Extraction Performance

To further observe the feature classification performance of the GCN-BiLSTM-Attention model, t-SNE dimensionality reduction was applied to visualize its outputs, revealing the classification effectiveness across different layers of the network. By combining datasets A, B, and C, we obtained dataset E comprising all samples. The original data distribution of dataset E is illustrated in Figure 9. It is evident that the two categories of data obtained through dimensionality reduction are relatively dispersed, lacking clear boundaries, and exhibit significant overlap. These overlapping regions correspond precisely to the areas where sample classification becomes challenging in transient stability assessments.

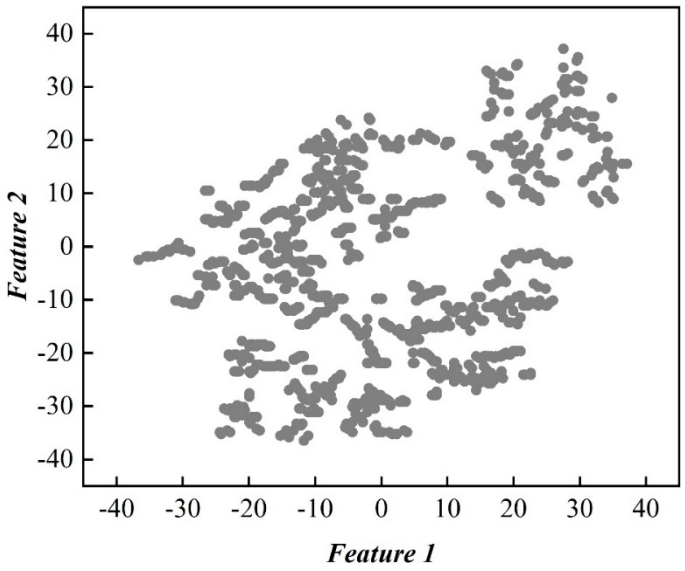

Figure 9. Original sample size is distributed.

Figure 10(a) and (b) show the hidden layer outputs of the BiLSTM-GCN and TA-BiLSTM layers in the GCN-BiLSTM-Attention network model, respectively. The distribution changes in features from Figure 9 to Figure 10 reveal that feature fusion through the BiLSTM-GCN layer integrates the topological characteristics of the power system with its temporal electrical features. As features aggregate, the boundary between the two data types becomes increasingly distinct, with overlapping areas progressively diminishing. Subsequently, as shown in Figure 10(b), the TA-LSTM layer extracts time-based transient characteristics from the fused features. This enables the GCN-BiLSTM-Attention model to capture more transient information, enhancing classification accuracy. The boundary between the two data types becomes distinctly clear, demonstrating the model's robust feature extraction capability and its potential for achieving effective transient stability assessment.

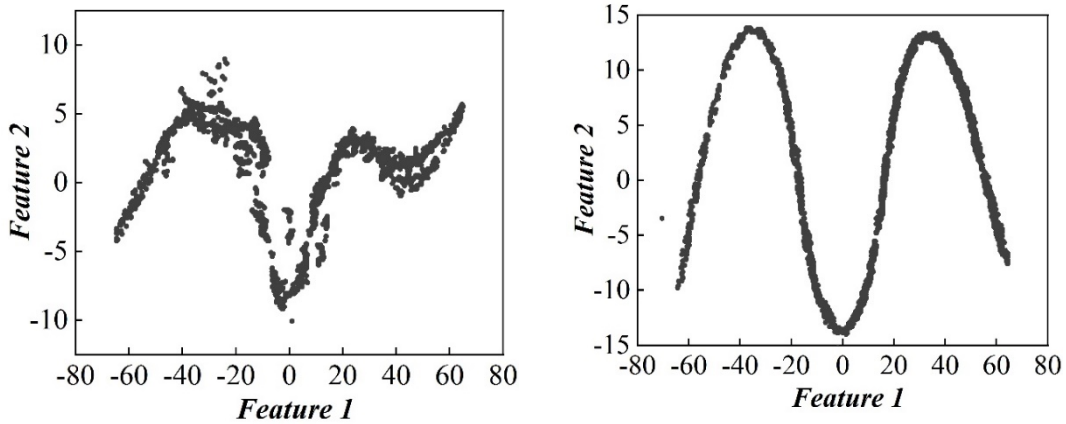

(a) BiLSTM-GCN **(b) TA-BiLSTM**

Figure 10. Data distribution visualization of different layers.

5. Conclusion

This paper addresses the challenge of monitoring and controlling grid voltage stability under high-density distributed power source integration by designing and constructing a dynamic early warning system based on Long Short-Term Memory (LSTM) networks. The main contributions and conclusions of this study are as follows:

(1) By leveraging BiLSTM and GCN coupled with attention mechanisms, this study captures both bidirectional temporal and spatial feature information of transient voltages. A spatiotemporal feature concatenation layer is constructed to comprehensively extract spatiotemporal characteristics of transient voltages, thereby enhancing the transient voltage stability assessment performance of the GCN-BiLSTM-based system for receiving-end grids.

(2) Reducing branch power enhances voltage stability in that branch. Reasonably adjusting DG power factor to minimize the transverse voltage drop component effectively improves system voltage stability.

(3) Performance comparisons against the baseline network model across the fully connected dataset A, N-1 outage dataset B, and N-2 outage dataset C validate the superior classification capabilities of the proposed Attention model. It achieves optimal metrics in accuracy, precision, recall, and F1 score. t-SNE dimensionality reduction visualizes the model's output across layers, revealing its data classification process.

(4) Future work may further optimize the layout and capacity of energy storage systems to enhance the grid's resilience against fluctuations from distributed power sources. Concurrently, strengthening coordination mechanisms among diverse power sources will better address varying electricity demands and challenges.

Funding

China Southern Power Grid limited liability company technology project, GZKJXM20222411, Research and demonstration of multi-time scale adaptive whole-area distribution network self-healing technology considering distributed resource carrying capacity (Subtopic 5).

References

1. Oliva, S., Muñoz, J., Fredes, F., & Sauma, E. (2022). Impact of increasing transmission capacity for a massive integration of renewable energy on the energy and environmental value of distributed generation. Renewable Energy, 183, 524-534.
2. Riaz, S., & Mancarella, P. (2021). Modelling and characterisation of flexibility from distributed energy resources. IEEE transactions on power systems, 37(1), 38-50.
3. Gill, A., Choudhary, A., & Bali, H. (2021). Renewable distributed generations optimal penetration in the distribution network for clean and green energy. Asian Journal of Water, Environment and Pollution, 18(2), 37-43.
4. Sha, A., & Aiello, M. (2018). Topological considerations on decentralised energy exchange in the Smart Grid. Procedia Computer Science, 130, 720-727.
5. Muhanji, S. O., Muzhikyan, A., & Farid, A. M. (2018). Distributed control for distributed energy resources: long-term challenges and lessons learned. IEEE Access, 6, 32737-32753.
6. Singh, S., & Singh, S. (2024). Advancements and challenges in integrating renewable energy sources into distribution grid systems: A comprehensive review. Journal of Energy Resources Technology, 146(9), 090801.
7. Wang, L., Yan, R., & Saha, T. K. (2019). Voltage regulation challenges with unbalanced PV integration in low voltage distribution systems and the corresponding solution. Applied Energy, 256, 113927.
8. Boyin, T., & Li'an, C. (2022, August). Research on the influence of distributed photovoltaic grid connection on voltage fluctuation. In 2022 Power System and Green Energy Conference (PSGEC) (pp. 267-271). IEEE.
9. Ahmadi, B., Ceylan, O., & Ozdemir, A. (2020, September). Impacts of load and generation volatilities on the voltage profiles improved by distributed energy resources. In 2020 55th International Universities Power Engineering Conference (UPEC) (pp. 1-6). IEEE.
10. Iweh, C. D., Gyamfi, S., Tanyi, E., & Effah-Donyina, E. (2021). Distributed generation and renewable energy integration into the grid: Prerequisites, push factors, practical options, issues and merits. Energies, 14(17), 5375.
11. Al-Ismail, F. S. (2020). Discussion on "A new formulation of distribution network reconfiguration for reducing the voltage volatility induced by distributed generation". IEEE Transactions on Power Systems, 35(6), 4974-4974.
12. Jeong, Y. C., Lee, E. B., & Alleman, D. (2019). Reducing voltage volatility with step voltage regulators: A life-cycle cost analysis of Korean solar photovoltaic distributed generation. Energies, 12(4), 652.
13. Talari, S., Shafie-Khah, M., Chen, Y., Wei, W., Gaspar, P. D., & Catalao, J. P. (2018). Real-time scheduling of demand response options considering the volatility of wind power generation. IEEE Transactions on Sustainable Energy, 10(4), 1633-1643.
14. Zhang, D., Li, J., & Hui, D. (2018). Coordinated control for voltage regulation of distribution network voltage regulation by distributed energy storage systems. Protection and Control of Modern Power Systems, 3(1), 1-8.

15. Fusco, G., & Russo, M. (2021). A decentralized approach for voltage control by multiple distributed energy resources. IEEE Transactions on Smart Grid, 12(4), 3115-3127.
16. Varetsky, Y., Fedorczak-Cisak, M., & Kushka, B. (2025). Studying Voltage Fluctuations in the MV Distribution Grid with a Renewable Energy Source. Energies, 18(16), 4217.
17. Medjroubi, W., Müller, U. P., Scharf, M., Matke, C., & Kleinhans, D. (2017). Open data in power grid modelling: new approaches towards transparent grid models. Energy Reports, 3, 14-21.
18. Li, L., Cai, Z., Tang, W., Zhang, Y., Zhang, J., Wu, Z., ... & Guan, L. (2022). Theoretical framework and key technologies of transparent power grid. Strategic Study of Chinese Academy of Engineering, 24(4), 32-43.
19. Xiaojing, W., Pengzhan, F., Hongbin, L., Wei, J., Zhechen, H., Yang, X., ... & Lei, W. (2023, October). Research on Transparent Support System of Distribution Grid Based on Digital Technology. In 2023 2nd Asian Conference on Frontiers of Power and Energy (ACFPE) (pp. 482-487). IEEE.
20. Chen, K., He, Z., Wang, S. X., Hu, J., Li, L., & He, J. (2018). Learning-based data analytics: Moving towards transparent power grids. CSEE Journal of Power and Energy Systems, 4(1), 67-82.
21. Bobinaite, V., Di Somma, M., Graditi, G., & Oleinikova, I. (2019). The regulatory framework for market transparency in future power systems under the web-of-cells concept. Energies, 12(5), 880.
22. Liu, B., Tan, Z., & Lan, C. (2022). Key concepts and framework of power distribution and utilization of transparent power grids. Frontiers in Energy Research, 10, 900890.
23. Ma, J., Wang, T., Shen, X., & Zhang, H. (2022, April). Survey of Distributed Transparent Access Control Platform in Power Grid. In 2022 IEEE Asia-Pacific Conference on Image Processing, Electronics and Computers (IPEC) (pp. 1030-1035). IEEE.
24. Alzaareer, K., & Saad, M. (2018, November). Real-time voltage stability monitoring in smart distribution grids. In 2018 International Conference on Renewable Energy and Power Engineering (REPE) (pp. 13-17). IEEE.
25. Dharmapala, K. D., Rajapakse, A., Narendra, K., & Zhang, Y. (2020). Machine learning based real-time monitoring of long-term voltage stability using voltage stability indices. IEEE Access, 8, 222544-222555. Ge, H., Guo, Q., Sun, H., & Zhao, W. (2020). A model and data hybrid-driven short-term voltage stability real-time monitoring method. International Journal of Electrical Power & Energy Systems, 114, 105373.
26. Wu, T., Zhang, Y. J. A., & Wen, H. (2020). Voltage stability monitoring based on disagreement-based deep learning in a time-varying environment. IEEE Transactions on Power Systems, 36(1), 28-38.
27. Lee, H., Srivastava, A. K., Krishnan, V. V., Niddodi, S., & Bakken, D. E. (2021). Decentralized voltage stability monitoring and control with distributed computing coordination. IEEE Systems Journal, 16(2), 2251-2260.
28. Cai, H., & Hill, D. J. (2022). A real-time continuous monitoring system for long-term voltage stability with sliding 3D convolutional neural network. International Journal of Electrical Power & Energy Systems, 134, 107378.
29. Villa-Acevedo, W. M., López-Lezama, J. M., Colomé, D. G., & Cepeda, J. (2022). Long-term voltage stability monitoring of power system areas using a kernel extreme learning machine approach. Alexandria Engineering Journal, 61(2), 1353-1367.
30. Xin, W. K., Liu, C. M., Rezaei-Zare, A., Li, A. Q., & Wang, Z. Z. (2023). Real-time monitoring method of power grid voltage stability during geomagnetic storms. IEEE Transactions on Power Delivery, 39(1), 192-201.
31. Amroune, M. (2021). Machine Learning Techniques Applied to On-Line Voltage Stability Assessment: A Review. Archives of Computational Methods in Engineering, 28(2).
32. Su, H. Y., & Lai, C. C. (2025). Improving Online Voltage Stability Monitoring in Smart Grids: A Physics-Informed Guided Deep Learning Model. IEEE Transactions on Industry Applications.
33. Zhang, M., Li, J., Li, Y., & Xu, R. (2021). Deep learning for short-term voltage stability assessment of power systems. IEEE Access, 9, 29711-29718.
34. Adhikari, A., Naetiladdanon, S., & Sangswang, A. (2022). Real-time short-term voltage stability assessment using combined temporal convolutional neural network and long short-term memory neural network. Applied Sciences, 12(13), 6333.
35. Mauricio Maca & Rosana Pérez. (2025). Classification of handwritten mathematical symbols with a BiLSTM network using a new online feature and permuting strokes. SeMA Journal,(prepublish),1-15.https://doi.org/10.1007/S40324-025-00407-6.